

DOI: 10.1002/sml.200500424

## Enhanced Secondary Electron Emission from Group III Nitride/ZnO Coaxial Nanorod Heterostructures\*\*

Shu Ping Lau,\* Lei Huang, Siu Fung Yu, Huiying Yang, Jin Kyoung Yoo, Sung Jin An, and Gyu-Chul Yi

Materials with a high secondary electron emission (SEE) yield ( $\sigma$ ) are valuable for vacuum devices, such as the protective layer of plasma displays,<sup>[1]</sup> radiation detectors,<sup>[2]</sup> and electron multipliers.<sup>[3]</sup> In SEE studies, an incident electron beam is used to produce secondary electrons inside a sample, and the yield and energy distribution of the secondary electrons emitted from the surface are analyzed to obtain information about the surface properties. It is known that the surface of group III nitrides (such as AlN, GaN) has a low or negative electron affinity (NEA) and is thus a promising material for high  $\sigma$  values.<sup>[4]</sup> Meanwhile,  $\sigma$  increases as the work function ( $\phi$ ) of the material decreases.<sup>[5]</sup> Therefore, one-dimensional (1D) nitride semiconductors have stimulated a great deal of interest for their application in cold cathode emitters, due to the combination of the NEA surface and a large field enhancement factor inherited from the nanostructure.<sup>[6]</sup> It has been demonstrated that group III nitride coatings are effective in improving the field-emission characteristics of Si-tip field-emitter arrays<sup>[7]</sup> and the electron-emission properties of GaN nanorod arrays.<sup>[6]</sup> Although these nanostructured electron emitters are being developed, in many cases the surface electronic properties of the nanostructured materials are not well understood.

Recently, it has been reported that MgO coated on aligned carbon nanotubes (CNTs) can produce a high SEE by applying a bias of 800 V, but the MgO coating was not coaxially grown on the sidewalls of the nanotubes. Thus, the coating lost the 1D feature of nanotubes, although the strong local field could still be generated by the tip of the

CNTs.<sup>[3]</sup> Besides CNTs, ZnO-based 1D nanostructures such as nanorods, nanowires, and nanoneedles have attracted considerable interest. Furthermore, the GaN/ZnO coaxial nanorod heterostructure has been demonstrated using a ZnO nanoneedle template followed by epitaxial growth of GaN.<sup>[8]</sup> Herein, we report the enhancement of SEE yields from ultrafine coaxial GaN/ZnO and AlN/ZnO nanoneedle heterostructures. It is found that the SEE yields are significantly enhanced by the inherited nanostructure from the ZnO nanoneedle template. The findings should shed light on the development of high-efficiency electron-emission devices, such as radiation detectors, based on the secondary electron effect of group III nitride nanostructured materials.

Figure 1 shows a schematic diagram of coaxial nanorod heterostructures and the experimental setup for measuring

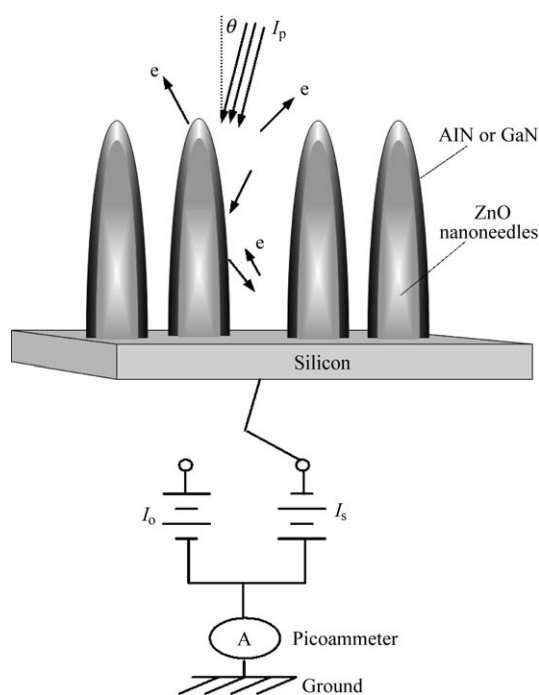


**Figure 1.** Schematic diagram of the coaxial heterostructure and the SEE experimental setup.  $\theta$  = angle of electron beam;  $I_p$  = primary beam current;  $I_0$  = sample-to-ground current of positively biased sample;  $I_s$  = sample-to-ground current of negatively biased sample.

[\*] Prof. S. P. Lau, Dr. L. Huang, Prof. S. F. Yu, H. Y. Yang  
School of Electrical and Electronic Engineering  
Nanyang Technological University  
Singapore 639798 (Singapore)  
Fax: (+65) 67933318  
E-mail: esplau@ntu.edu.sg

J. K. Yoo, S. J. An, Prof. G.-C. Yi  
National CRI Center for Semiconductor Nanorods  
Department of Materials Science and Engineering  
Pohang University of Science and Technology (POSTECH)  
Pohang, Gyeongbuk 790-784 (Korea)

[\*\*] This work was supported by NTU RGM 17/04, the National Creative Research Initiative Project, and the Center for Nanostructured Materials Technology under the 21st Century Frontier R&D Program of the Ministry of Science and Technology, Korea.

$\sigma$ . The procedure was carried out in a scanning electron microscope by measuring the specimen current after biasing the specimen in two separate experiments.<sup>[10–12]</sup> The surface morphology of ZnO nanoneedles, and of AlN/ZnO and GaN/ZnO coaxial heterostructures, was investigated by SEM. The as-grown vertically aligned ZnO nanoneedles have sharp tips (see Figure 2a). A low-magnification transmission electron microscopy (TEM) image of an individual ZnO nanoneedle with a diameter of about 40 nm in the stem is presented in Figure 2b. Figure 2c shows a high-resolution TEM (HRTEM) image of a ZnO nanoneedle measured along the stem. The lattice spacing of approximately 2.6 Å between adjacent lattice planes corresponds to the distance between two (002) crystal planes, which confirms

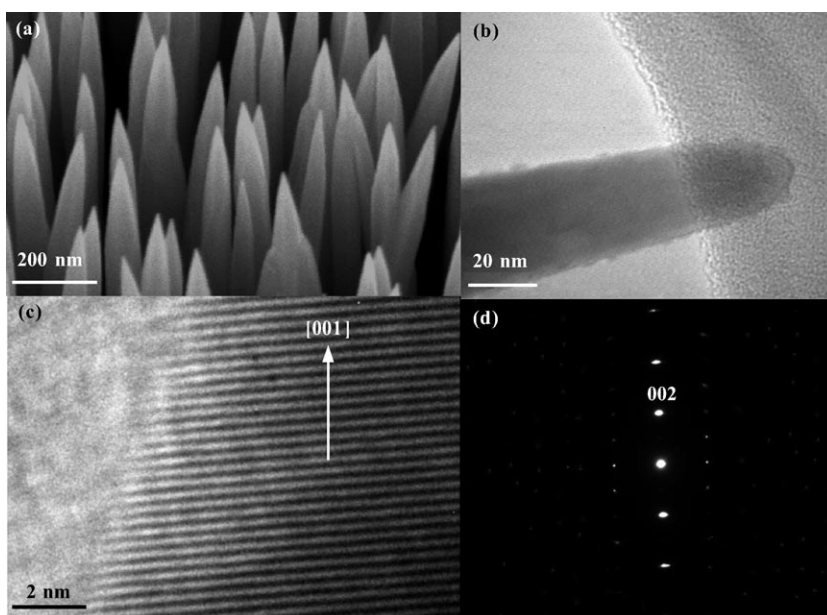


**Figure 2.** a) Scanning electron microscopy (SEM) image of vertically aligned ZnO nanoneedles. b) TEM image showing an individual ZnO nanoneedle. c) Lattice-resolved image and d) SAED pattern confirming the single-crystal nature of the ZnO nanoneedle. Growth occurs along the [001] direction.

[001] as the preferred growth direction for ZnO nanoneedles. The corresponding selected-area electron diffraction (SAED) pattern of the nanoneedle shows a single-crystal hexagonal structure (Figure 2d).

As compared to the ZnO nanoneedles, the AlN/ZnO and GaN/ZnO coaxial heterostructures exhibit flat tip ends instead of the original sharp tips (Figures 3a and 4a). The AlN and GaN layers are not only deposited on the tips of ZnO nanoneedles but also uniformly coated along the sidewall of the ZnO-core nanoneedles, as shown in the TEM images of Figures 3b and 4b, respectively. The estimated thickness of the AlN and GaN layers coated on ZnO nanoneedles was about 10 nm. As shown in Figure 3c, the HRTEM image of an AlN/ZnO coaxial heterostructure shows an abrupt interface between the AlN and ZnO layers. The corresponding SAED pattern (Figure 3d) displays rings from the randomly oriented polycrystalline AlN hexagonal structure and single-crystal spots of ZnO. The HRTEM image (Figure 4c) and the corresponding SAED pattern (Figure 4d) of a GaN/ZnO coaxial heterostructure verify that GaN layers are epitaxially grown on ZnO nanoneedles. The SAED pattern shows double spots, which can be

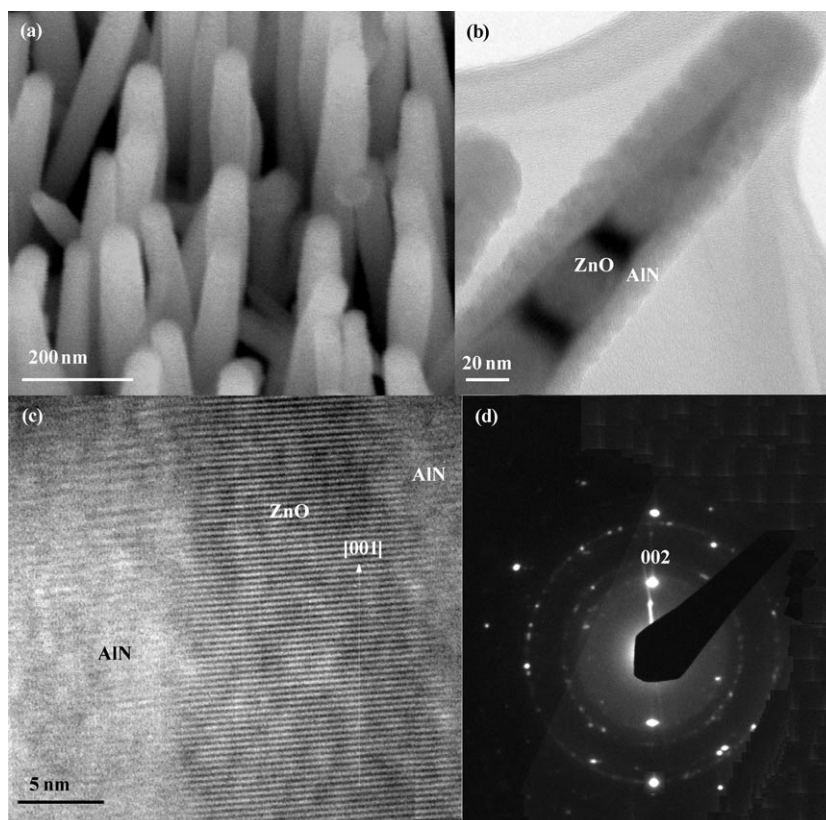


**Figure 3.** a) SEM image of an AlN-coated ZnO nanoneedle coaxial heterostructure. b) TEM image showing a single AlN/ZnO heterostructure. c) HRTEM image showing the interface of AlN and ZnO. d) SAED pattern of the AlN/ZnO heterostructure confirming the polycrystalline and single-crystal nature of AlN and ZnO, respectively.

indexed as a [100] zone axis of wurtzite GaN and ZnO. The lattice fringes of GaN can be clearly observed in Figure 4c after the specimen was tilted to a certain angle. In comparison to the AlN/ZnO heterostructure, GaN/ZnO exhibited better crystal quality, which may be due to the relatively smaller lattice mismatch between GaN and ZnO (1.8%) than between AlN and ZnO ( $\approx 4\%$ ). Both the AlN and GaN films on Si substrates exhibited polycrystalline structures, as evidenced by cross-sectional TEM (not shown).

Prior to the yield measurement, atomic force microscopy (AFM; NanoScope IIIa, Digital Instruments) studies were performed on all the specimens. The separation between the individual coated nanoneedles is estimated to be in the range of 200 to 300 nm from the peak-to-peak distance of the depth profiles in the 3D AFM topography images (not shown). The root-mean-square (rms) roughness of the AlN/ZnO heterostructure is 75.5 nm, which is almost twice of that of the GaN/ZnO coaxial heterostructure (39.1 nm). The films deposited on Si substrates are

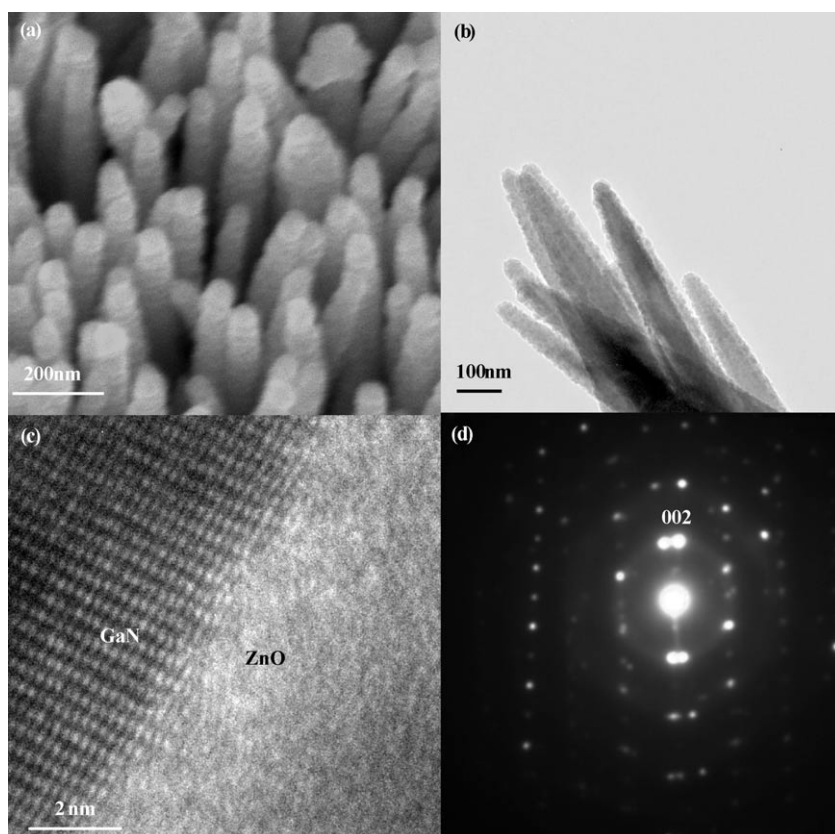


**Figure 4.** a) SEM image of a GaN-coated ZnO nanostructure. b) TEM image showing the uniformly coated GaN/ZnO heterostructure. c) Lattice-resolved image of GaN confirming its single-crystal nature. d) SAED pattern with spot splitting, as GaN and ZnO have slightly different lattice constants.

mirrorlike smooth. The rms roughness of the AlN and GaN films is 4.1 and 3.3 nm, respectively. Thus, the roughness feature of the AlN/ZnO and GaN/ZnO coaxial heterostructures is mainly inherited from the vertically aligned ZnO nanoneedle templates.

Figure 5 shows  $\sigma$  as a function of primary electron energy on all the samples. Interestingly, AlN- and GaN-coated ZnO nanoneedles have a much higher  $\sigma$  value than those deposited on Si substrates. In particular, the  $\sigma$  values of AlN/ZnO and GaN/ZnO coaxial heterostructures for the primary electron energy from 0.8 to 20 keV are always larger than 1. The peak values are more than 6, which is up to 1.6 and 2.1 times larger than those of AlN and GaN thin films on Si, respectively, under the same deposition conditions. In addition, the  $\sigma$  value decreases rapidly to about one-third of its maximum value as the incident electron energy increases. The  $\sigma$  value of the ZnO nanoneedle template is also included in Figure 5 for comparison. It is observed that the yield is around 1 for the primary electron energy ranging from 0.8 to 20 keV. These results suggest that the enhancement of the SEE in the coaxial heterostructure is due to the combined effect of the group III nitride layer and nanostructured topography. Also, the enhancement of the SEE does not seem to depend on the crystal quality of the nitride layer, as the AlN/ZnO heterostructure

showed stronger SEE enhancement than the GaN/ZnO heterostructure, even though the AlN layer was only polycrystalline. In addition, the nanoneedles cause a dispersion of the incidence angle of primary electrons. Considering the normal incidence on the sidewall of nanoneedles, this effect results in a higher  $\sigma$  value due to the increase of SEE with inclined incidence.<sup>[11]</sup>

The  $\sigma$  value was measured on all the samples for incidence angles ( $\theta$ ) of the electron beam varying from  $0^\circ$  to  $60^\circ$ , to investigate the effect of the nanostructured topography on the SEE. The angle  $\theta$  is defined in Figure 1. A power law relationship has been successfully employed to explain the SEE properties of the surface of amorphous materials. The total penetration depth  $d$  of an electron beam is directly proportional to  $E_p^n$ , where  $E_p$  is the primary electron energy and  $n$  is a material-dependent exponent.<sup>[13]</sup> According to the power law, the relationship between the SEE yield  $\sigma_\theta$  (the value of  $\sigma$  for a given incidence angle  $\theta$ ) and the angle  $\theta$  of the electron beam can be described by Equation (1)

$$\ln(\sigma_\theta) = k(1 - \cos\theta) + a \quad (1)$$

where  $k$  and  $a$  denote the gradient and  $y$  intercept of the plots between  $\ln(\sigma_\theta)$  and  $(1 - \cos\theta)$ , respectively.<sup>[11,13]</sup>

Figure 6 shows the plots of  $\ln(\sigma_\theta)$  against  $(1 - \cos\theta)$  at low primary electron energies ( $\leq 2$  keV). As expected, the data of the films deposited on Si substrates can be fitted by a straight line for the entire energy range, which is similar to the observation from SiO<sub>2</sub> reported by Yong et al.<sup>[11]</sup> However, the data of the coaxial heterostructures do not follow the power law relationship; the plots show a discontinuity, and two linear fits with different slopes are required for the two regions of incidence angles  $\leq 20^\circ$  and  $> 20^\circ$ . This result may be due to the fact that the nanostructured topographic surfaces have a significant effect on the SEE properties, which leads to the disagreement with the power law. According to the fitting results of plots of  $\ln(\sigma_\theta)$  against  $(1 - \cos\theta)$  (Figure 6), the values of  $k$  at different primary electron energies are as summarized in Table 1. There are two linear fits for coaxial heterostructure samples, and  $k_1$  and  $k_2$  are the gradients of fits for low ( $\leq 20^\circ$ ) and high incidence angles ( $> 20^\circ$ ), respectively. For the films deposited on Si substrates, the values of  $k$  (0.72 to 1.25) are comparable with the work on SiO<sub>2</sub> at electron energies ranging from 0.8 to 2 keV.<sup>[11]</sup> However, for the coaxial heterostructures, the values of  $k_1$  are almost one order of magnitude larger than those of  $k_2$ , which indicates that there are more increments of  $\sigma_\theta$  at low incidence angles ( $\leq 20^\circ$ ) than at the higher incidence angles ( $> 20^\circ$ ). In addition, the values of  $k_2$

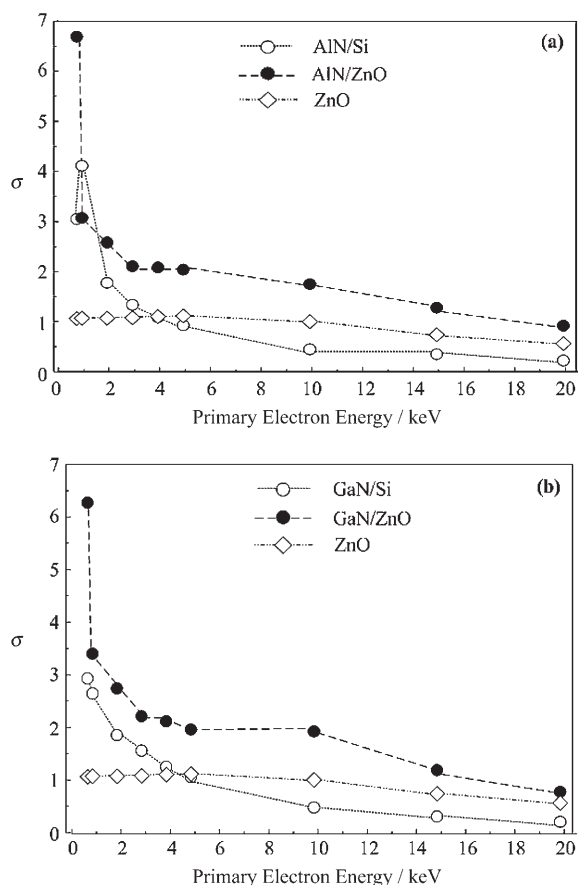


**Figure 5.** Plots of  $\sigma$  as a function of primary electron energy from a) an AlN thin film on Si and an AlN/ZnO heterostructure and b) a GaN thin film on Si and a GaN/ZnO heterostructure. The data for ZnO nanoneedles are included as reference.

are increased with increasing primary electron energy, which is similar to the case of the films deposited on Si substrates. However, it is observed that the values of  $k_1$  decrease with increasing primary electron energy.

The dependence of SEE on incidence angle for the coaxial heterostructures is related to the nanostructured topographic surface of the vertically aligned heterostructures. For a low-tilt incidence angle ( $\leq 20^\circ$ ), the incidence on the sidewall of the coaxial heterostructures causes an enhancement of the inclined-incidence effect. Moreover, a number of backscattering electrons may re-enter and penetrate the next part of the protrusions to produce new secondary electrons that can escape from the other surface. Therefore, the enhanced inclined-incidence effect and the re-enter/re-emission effect lead to more SEE and result in higher  $k_1$  values

**Table 1.** Gradients of  $\ln(\sigma_\theta)$  against  $(1-\cos\theta)$  as a function of primary electron energies.

Primary electron energy [keV]	AlN/ZnO		AlN/Si	GaN/ZnO		GaN/Si
	$k_1$	$k_2$	$k$	$k_1$	$k_2$	$k$
0.8	3.39	0.31	0.82	2.01	0.25	0.72
1	3.31	0.34	0.89	2.00	0.30	0.82
2	2.75	0.58	1.25	1.85	0.49	1.10

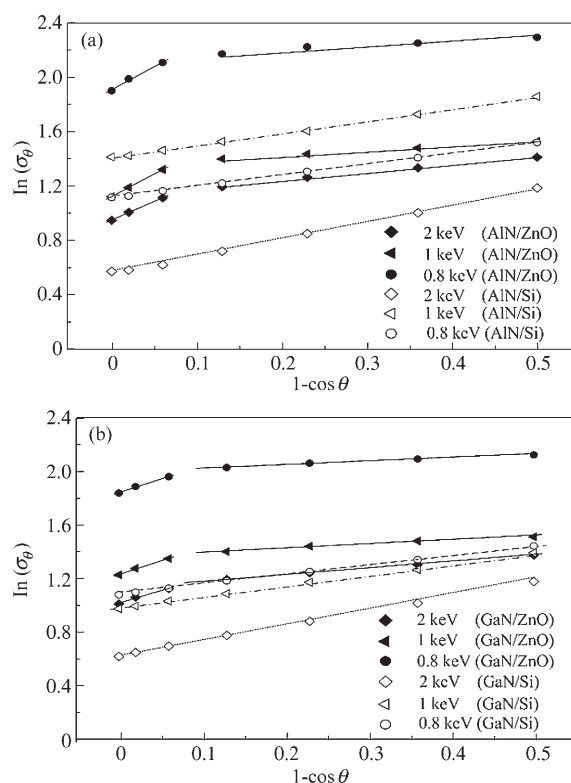


**Figure 6.** Plots of angular dependence of  $\ln(\sigma_\theta)$  against  $(1-\cos\theta)$  for a) an AlN thin film on Si and an AlN/ZnO heterostructure and b) a GaN thin film on Si and a GaN/ZnO heterostructure.

in the range of low-tilt incidence angles ( $\leq 20^\circ$ ). If the incidence angle is further tilted ( $> 20^\circ$ ), the inclined-incidence effect and the re-enter/re-emission effect still keep a slight increase in SEE yield  $\sigma_\theta$  with increasing tilt incidence angle. However, Figure 1 indicates that the SEE from the bottom of the nanostructured surface may not escape from the surface and contribute negatively to the SEE yield, which leads to relatively smaller  $k_2$  values in the range of high-tilt incidence angles ( $> 20^\circ$ ). The length of the nanoneedles was measured to be around 700–800 nm. Thus, a critical incidence angle of  $18.4^\circ$  is estimated for a wider range of lengths ( $L$ ) and separations ( $S$ ) using values such as  $L = 750$  nm and  $S = 250$  nm. This result suggests that the shadow effect may lead to restraining of the SEE from the bottom of the nanostructured surface if the incidence angles are larger than  $18.4^\circ$ . Notably, the estimated critical incidence angle is close to  $20^\circ$ . Therefore, the study of the dependence of SEE on incidence angle for the nanostructured topographic surface is important. The inclined-incidence and re-enter/re-emission effects together could enhance the SEE.

Both the effects are related to the aspect ratio of nanostructures, areal density, and nanostructured topographic configuration. Thus, the slight difference in the performance of SEE for AlN/ZnO and GaN/ZnO coaxial heterostructures may be at-

tributed to the difference in nanostructured topography. The findings should shed light on the development of highly efficient electron-emission devices, such as radiation detectors, based on the secondary electron effect of group III nitride nanostructured materials.

In conclusion, AlN/ZnO and GaN/ZnO coaxial heterostructures have a higher SEE yield than thin films of AlN and GaN deposited on Si substrates. The dependence of the SEE on incidence angle indicates that AlN/ZnO and GaN/ZnO coaxial heterostructures do not follow the power law, unlike the films deposited on Si substrates. The  $\sigma$  value of the heterostructures was enhanced significantly by the inherited nanostructures from the ZnO nanoneedle templates. These results suggest that the enhancement of SEE in the coaxial heterostructures is due to the combined effect of the group III nitride layer and the nanostructured topography.

### Experimental Section

ZnO nanoneedles were grown by catalyst-free metal-organic vapor-phase epitaxy (MOVPE) on Si substrates using diethylzinc ( $\text{Et}_2\text{Zn}$ ) and oxygen gas in the 400–500 °C range.<sup>[9]</sup> Then, an AlN or GaN layer 10 nm in thickness was deposited on the ZnO nanoneedles using trimethylaluminum and trimethylgallium as precursors, respectively. Details of the growth conditions and structural characterizations of the coaxial heterostructures have been reported elsewhere.<sup>[8]</sup>

The measurement of  $\sigma$  was carried out in a scanning electron microscope (JEOL JSM-5910LV) by measuring the specimen current after biasing in two separate experiments.<sup>[10–12]</sup> A 45-V batteries box was used for the sample biasing. The sample-to-ground current was measured with a low-noise current preamplifier (Stanford Research Systems, SR570). The electron beam was generated by the electron gun of the microscope. The beam current ( $I_p$ ) was measured by a Faraday cup attached to the SEM system and fixed at 100 pA by adjusting the spot size when the electron-beam energy was varied from 0.8 to 20 keV. In the first measurement, the sample was positively biased (+45 V) and the sample-to-ground current ( $I_0$ ) was measured for a selected primary-beam energy. The positive bias was adequate to insure

complete electron collection, so that  $I_0$  was the total incident electron current. Subsequently, the sample-to-ground current ( $I_s$ ) was measured as the sample was biased at a negative voltage (–45 V) to repel the secondary electrons from the sample surface. The difference in sample-to-ground currents measured under the different conditions was taken as the SEE. Thus, [Eq. (2)]

$$\sigma = (I_0 - I_s)/I_0 \quad (2)$$

### Keywords:

heterostructures • nanorods • nitrides • secondary electron emission • semiconductors

- [1] T. J. Vink, R. G. F. A. Verbeek, V. Elsbergen, P. K. Bachmann, *Appl. Phys. Lett.* **2003**, *83*, 2285.
- [2] J. Cazaux, *J. Appl. Phys.* **2001**, *89*, 8265.
- [3] W. S. Kim, W. Yi, S. Yu, J. Heo, W. Yi, S. Yu, J. Heo, T. Jeong, J. Lee, C. S. Lee, J. M. Kim, H. J. Jeong, Y. M. Shinm, Y. H. Lee, *Appl. Phys. Lett.* **2002**, *81*, 1098.
- [4] C. I. Wu, A. Kahn, *Appl. Surf. Sci.* **2000**, *162–163*, 250.
- [5] R. A. Baragiola, E. V. Alonso, J. Ferron, A. O. Florio, *Surf. Sci.* **1979**, *90*, 240.
- [6] H. M. Kim, T. W. Kang, K. S. Chung, J. P. Hong, W. B. Choi, *Chem. Phys. Lett.* **2003**, *377*, 491.
- [7] R. W. Pryor, *Appl. Phys. Lett.* **1996**, *68*, 1802.
- [8] S. J. An, W. I. Park, G. C. Yi, Y. J. Kim, H. B. Kang, M. Kim, *Appl. Phys. Lett.* **2004**, *84*, 3612.
- [9] W. I. Park, G. C. Yi, M. Kim, S. J. Pennycook, *Adv. Mater.* **2002**, *14*, 1841.
- [10] H. Padamsee, A. Joshi, *J. Appl. Phys.* **1979**, *50*, 1112.
- [11] J. C. Yong, J. T. L. Thong, J. C. H. Phang, *J. Appl. Phys.* **1998**, *84*, 4543.
- [12] A. Hoffman, S. Praver, R. Kalish, *Phys. Rev. B* **1992**, *45*, 12736.
- [13] M. Salehi, E. A. Flinn, *J. Appl. Phys.* **1981**, *52*, 994.

Received: November 2, 2005

Revised: January 25, 2006

Published online on April 7, 2006